HHS Public Access

Author manuscript

ASAIO J. Author manuscript; available in PMC 2018 January 01.

Published in final edited form as:

ASAIO J. 2017 ; 63(1): 14–23. doi:10.1097/MAT.0000000000000443.

LVAD Outflow Graft Angle and Thrombosis Risk

Alberto Aliseda[1], **Venkat Keshav Chivukula**[1], **Patrick McGah**[1], **Anthony R. Prisco**[2], **Jennifer A. Beckman**[3], **Guilherme J.M. Garcia**[2], **Nahush A Mokadam**[4], and **Claudius Mahr**[3]

[1]Department of Mechanical Engineering, University of Washington, Seattle, WA, USA

[2]Biotechnology and Bioengineering Center, Medical College of Wisconsin, Milwaukee, WI, USA

[3]Division of Cardiology, University of Washington, Seattle, WA, USA

[4]Division of Cardiothoracic Surgery, University of Washington, Seattle, WA, USA

Abstract

This study quantifies thrombogenic potential of a wide range of LVAD outflow graft anastomosis angles through. This study aims at clarifying the influence of a single parameter (outflow graft angle) on the thrombogenesis associated with flow patterns in the aortic root after LVAD implantation. This is an important and poorly-understood aspect of LVAD therapy, because several studies have shown strong inter-and intra-patient thrombogenic variability and current LVAD implantation strategies do not incorporate outflow graft angle optimization. Accurate platelet-level investigation, enabled by statistical treatment of outliers in Lagrangian particle tracking, demonstrate a strong influence of outflow graft anastomoses angle on thrombogenicity (platelet residence times and activation state characterized by shear stress accumulation) with significantly reduced thrombogenic potential for acutely-angled anastomosed outflow grafts. The methodology presented in this study provides a device-neutral platform for conducting comprehensive thrombogenicity evaluation of LVAD surgical configurations, empowering optimal patient-focused surgical strategies for long-term treatment and care for advanced heart failure patients.

Keywords

left ventricular assist devices; thrombogenic risk; outflow graft; flow patterns; residence time; platelet shear stress history; Lagrangian tracking

1 INTRODUCTION

Heart failure (HF) afflicts 2.4% of the US population (> 5 million) and over 500,000 new cases are reported annually. Medical treatment costs for HF-related cases exceeded $30 billion in 2012[1]. The prevalence of HF increases with age and, staggeringly, ~50% of patients diagnosed with HF die within 5 years[1]. Furthermore, the prevalence of HF is projected to increase to > 8 million people by 2030, with the total annual cost of HF care increasing to a projected $70 billion[2–4]. Medical-therapy refractory advanced heart failure

Corresponding Author: Alberto Aliseda (aaliseda@uw.edu).

Disclaimers: None

(ACC/AHA Stage D), comprises approximately 5 – 10% of the HF population[1,5] and is characterized by intolerance to neurohormonal therapy[6]. Heart transplant is the treatment of choice for end-stage HF patients; however, that option is limited by a severe shortage of suitable donor organs and thus remains epidemiologically insignificant[3,7]. Consequently, mechanical circulatory support with left ventricular assist devices (LVAD) has emerged as a viable long-term option for patients with medical-therapy refractory heart failure. The implantation rate of LVADs has tripled over the previous decade[8,9], largely driven by improved designs and reliability and associated greatly enhanced survival and quality of life for end-stage HF patients: 1-year survival rates for LVAD patients are now approaching 90%[3,10–13]. LVAD patients, however, remain at elevated risk for devastating complications like cerebrovascular events (stroke) and device thrombosis[11,12, 14–16]. As such, investigations into optimizing VAD configurations to reduce complication rates are imperative[3,7,17].

Despite significant advancements in LVAD design and development, the basic implantation technique has remained largely unchanged: the pump is connected to the left ventricle via an inflow cannula, and to the systemic circulation via an outflow graft typically anastomosed to the ascending aorta, proximal to the brachiocephalic artery and distal to the aortic sinus.

Neurologic events remain the most devastating complications of LVAD support[12,15, 18–21]; thus, despite advancements in LVAD technology and anti-coagulation therapy, it is imperative to examine the thrombogenicity of VAD configurations. As blood flow in the outflow graft and great vessels is characterized by high Reynolds, O(1000), and Womersley, O(10), numbers, the nuances of surgical implantation configuration may impact hemodynamic patterns, which in turn determine stress levels on endothelial and blood-suspended cells. Thrombogenesis in LVADs is attributable to several mechanisms such as the presence of non-biologic material in the blood path, non-physiological blood flow leading to red blood cell damage, endothelial dysfunction and platelet activation[12,14, 22–24]. Significant research efforts have been dedicated to modeling hemodynamics in the LVAD outflow graft using computational fluid dynamics (CFD) and other tools[25–33]. These studies focus on Eulerian parameters, i.e. wall shear stress (WSS), that are essential to understanding endothelial mechanotransduction but characterize the complex hemodynamics experienced by blood-suspended cells incompletely. Additionally, some of the early work had methodological limitations, associated with available tools at the time. For example, most studies assumed steady-state flow conditions. Flow in the aortic arch and great vessels is inherently unstable due to high Reynolds numbers and complex geometry (curvature, branch bifurcations, etc.) and thus unsteady, and frequently chaotic, even for continuous flow LVAD support with minimal native contribution to cardiac output. Modern computational and experimental techniques, along with more powerful computing hardware, have opened the doors to studying hemodynamics of the LVAD outflow graft in its natural unsteady, chaotic, and patient-specific complexity.

Lagrangian metrics, shear stress history and residence time computed from particle tracking, are ideally suited to evaluate platelet activation. This study focuses on rigorously measuring LVAD thrombogenic potential by computing stress-time variables that have been shown to correlate strongly to platelet activation/accumulation in a reference frame that follows blood-

suspended particles/cells. A combination of Lagrangian (particle-tracking) metrics with traditional Eulerian wall shear stress maps is evaluated for different LVAD outflow graft anastomoses angles in order to describe the relative risk assessment of thrombogenic potential, laying the groundwork for outflow graft optimization in a patient-specific context.

We hypothesize that VAD outflow graft angle impacts transport of blood-suspended cells, and shear stress acting on both blood and arterial endothelium. The existence of chaotic trajectories and associated shear stress affects platelet activation, platelet-endothelium and platelet-platelet signaling, and ultimately leads to incipient conditions for thrombus formation. Our objective is to elucidate the influence of surgical VAD outflow graft configurations on thrombogenic factors. With the aid of state-of-the-art techniques such as 3D patient-specific models, virtual surgery, unsteady CFD and Lagrangian particle tracking, this study analyzes the thrombogenic potential for various LVAD outflow graft anastomoses configurations. In Section 2, we describe in detail the development of a patient-specific LVAD model, virtual surgical implantation of outflow grafts at different angles on the aortic arch, and the CFD simulation of flow and particle transport (Eulerian-Lagrangian) in the outflow graft, aortic arch and great vessels of the brain. Comparisons of the thrombogenic metrics computed for various LVAD outflow graft anastomoses are presented in Section 3, followed by an in-depth discussion of technological and clinical implications of the results. The methodology developed in this work is general and employs a device-neutral approach, which will enable designing LVAD implantation strategies in a patient-specific manner over a wide range of conditions.

2 METHODS

The methodology developed to evaluate the thrombogenic potential of LVAD outflow graft implantation at different angles is based on a 3D patient-specific model of the aorta, an LVAD outflow graft that is implanted through virtual surgery, and CFD simulation of the blood flow in the aortic territory.

2.1 Patient-specific model of the aortic arch and great vessels

Gadolinium-enhanced magnetic resonance angiography (MRA) was performed on a 25 year old male[34] to image the vasculature of the ascending aorta and great vessels after having necessary permissions and consent.

Image segmentation was performed using the SimVascular software package (https://simtk.org) to delineate the aortic arch, descending aorta (DA) and the major blood vessels of the aorta, namely the brachiocephalic (B), left subclavian (S) and common carotid (CCA) arteries. A 3D surface was reconstructed from the segmented vessel outlines in Solidworks (Solidworks®, Dassault Systems, France) and transferred in STL (see Figure 1) format to the CFD mesh generation software.

2.2 Virtual surgical implantation of the LVAD outflow graft

Using virtual surgery, we “implanted” a 10-mm diameter LVAD outflow graft on the ascending aorta, distal to the aortic root and proximal to the brachiocephalic artery. Three different outflow graft configurations were created by anastomosing the LVAD outflow graft

at 45°, 60° and 90° with respect to the axis of the ascending aorta (see Figure 1). The graft was assumed to be rigid and, therefore, the cross sectional area and the angle with the aorta remained unchanged to dilatation of the graft under pressure and unaffected by the remote possibility of long-term remodeling.

2.3 Mesh generation and CFD simulations

The virtually-anastomosed aortic arch/outflow graft models were imported into the meshing software Gambit (ANSYS Inc., Canonsburg, PA) and tetrahedral unstructured meshes created for all three configurations. The meshes contained upwards of 5 million cells with a typical spacing between nodes of ~100 microns. Discretization of the computational domain with high spatial density is required to capture the transitional or chaotic flow in the aortic arch ($Re_{peak} > 3000$). The time step was set at 10^{-4} s to provide sufficient temporal resolution to resolve all unsteady motions in the flow. This mesh density was satisfactorily evaluated for grid independence, including a volumetric estimate of viscous dissipation that accurately captured energy balance between the inlets, outlets and within the fluid domain with shear being fully resolved spatially and temporally in the simulation. The meshes were then imported into the CFD simulation software (FLUENT, ANSYS Inc., Canonsburg, PA) to set boundary conditions.

The CFD simulations in this work include two distinct fluid phases: a continuous phase where the blood is modeled as a homogeneous Newtonian fluid, and a discrete phase where the platelets are modeled as neutrally-buoyant particles transported by the continuous phase. The underlying governing equations and fluid properties are provided in the supplementary materials. All simulations were performed on a distributed-memory massively parallel architecture facility (Hyak HPC) at the University of Washington.

2.4 Lagrangian particle tracking

Once the hemodynamics of the continuous phase was computed, Lagrangian particle tracking was implemented for the discrete phase. Hundreds of thousands of particles with a diameter of 3 microns were released from the LVAD outflow graft inlet (see Figure 2).

2.4.1 Particle trajectories—The particle trajectories were constructed from their location at each fluid time step, from particle injection at the outflow graft to particle exit through any of the vessels: brachiocephalic, subclavian, carotid or descending aorta, or to their final positions if they remain in the aortic territory.

2.4.2 Particle residence time (RT)—The particle residence time (RT) was calculated by tracking the time each particle remained in the vascular domain:

$$\boldsymbol{RT}_i = T_i^{\text{entrance}} - T_i^{\text{exit}} \quad (1)$$

Where i is an index for each particle, T_i^{entrance} represents the time the particle is injected into the domain, and T_i^{exit} represents the time the particle trajectory ends.

2.4.3 Particle stress history (SH)—Platelet activation triggers the coagulation cascade[35] and ultimately may lead to thrombus formation. While many factors influence platelet activation, one of the most widely accepted theories is shear-induced-platelet-activation (SIPA)[12,36–40]. Lagrangian tracking allows for determination of accumulated shear stress on each platelet, as a function of time in the flow, to evaluate the level of SIPA associated with each LVAD outflow graft angle studied:

$$SH = \int_{t_0}^{t} \tau(\boldsymbol{X}(t'), t')dt' \quad (2)$$

Where τ is the instantaneous shear stress magnitude at time t' and $X(t')$ is the platelet's location at that time.

2.5 Model Boundary Conditions

The inflow of blood through the LVAD outflow graft, set to 5 l/min, constituted the only inlet in this simulation. Two-element Windkessel models with physiologically-realistic vascular resistances and capacitances[54] (see Supplementary Materials for details) were applied at each of the four outlets (i.e. brachiocephalic, carotid, subclavian and descending aorta).

The aortic valve was assumed to remain closed to simplify analysis of the outflow graft anastomosis in this paper, representing a fully unloaded patient for whom cardiac output solely originates from VAD support. All arterial walls were considered no-slip walls. All simulations were initialized for a period of 2–3 seconds to reject the initial transient that develops in the computational domain; valid data collection for particles and global parameters (WSS) was initiated after exclusion of this initial transient and simulations were performed for a minimum of 10 equivalent cardiac cycles (t >10 s).

2.6 Evaluation of minimum thrombogenic potential (MTP)

A thrombogenic potential (TP) was defined based on a combination of weighted statistical Lagrangian measures of the RT and SH distributions among platelets, as shown in Table 1. Specifically, statistics of particle RT and SH were analyzed using median and outlier information. This analysis was motivated by the strong link between particle RT, accumulation of shear stress history and SIPA, which initiates coagulation. The value of MTP is meant to rank-order the thrombogenic potential of each particular LVAD outflow graft configuration, reducing the complex data provided by the simulation to one single metric with arbitrary units, but not to evaluate an absolute risk of thrombosis (that is a value of 1 represents higher risk than 0.5, but does not mean that there is 100% probability of thrombosis, nor that the probability is twice as high as 0.5). All statistical analyses were conducted in MATLAB (MathWorks Inc., Natick, MA), and the non-parametric Wilcoxon rank-sum test with a 95% confidence interval ($p < 0.05$) was used for all significance evaluations, owing to the highly right-skewed nature of particle data.

Residence and shear statistics are presented using (i) boxplots (denoting median, range and outliers), (ii) probability density functions (PDF) and (iii) probability of occurrence (PO).

The PO metric enables determination of the probability that a particle selected at random has a specific RT or has accumulated a specific SH. These enabled the investigation of particle RT and SH distributions for various configurations to determine platelets with highest risk of activation, and incorporated into the evaluation of TP.

3 RESULTS

Global hemodynamic parameters (WSS) and particle trajectories, RT, SH and TTP were computed for each outflow graft angle configuration. MTP was evaluated from the collective blood-suspended and vascular wall mechanical and transport statistics. Results for Lagrangian particle tracking analyses are presented first, followed by global hemodynamic parameters and MTP evaluation.

3.1 Lagrangian metrics for evaluating thrombogenicity

3.1.1 Blood flow patterns—Hemodynamic flow patterns of blood entering the aortic arch from the outflow graft are shown in Figure 3 for the 60° and 90° outflow graft configurations. The high-velocity jet from the outflow graft impinges on the contralateral aortic wall forming a stagnation region, with high pressure and low shear stress at the stagnation point surrounded by concentric rings of decreasing pressure and very high shear stress. The 90° configuration is the most adverse, with the outflow jet perpendicular to the aortic axis, resulting in a strong recirculation flow pattern. This is clearly seen in Figure 3(b), where multiple pathlines spiral out from the stagnation point and traverse the anatomy of the ascending aorta and aortic arch. A significant recirculating region appears at the aortic root, just distal of the aortic valve, with associated low shear and high cell residence times just following the high shear associated with the jet and wall impingement.

Figure 4 shows snapshots of particles at 1 and 2 seconds after being injected at the outflow graft anastomosis for the 60° and 90° configurations. For the 90° angle configuration, one second after injection more than 80% of the particles are still circulating in the ascending aorta, aortic arch, proximal segments of the great vessel and descending aorta region. This compares negatively to fewer than 20% of particles still circulating for the 60° angle configuration, indicating a higher risk of particles in the 90° configuration to accumulate higher stress history, increasing activation risk.

3.1.2 Platelet trajectories—Figure 5 shows characteristic platelet trajectories, from injection at the outflow graft, for all three configurations. Trajectories are plotted for ~ 30 particles exiting through each of the brachiocephalic (blue), left common carotid (red) and left subclavian (green) arteries. It can be observed that the paths traversed by the platelets are very different for the three configurations studied. Qualitatively, the 90° configuration (Figure 5(c)) clearly results in a larger number of trajectories following more circuitous routes through the aortic arch and towards the distal vessels. These will be quantified rigorously with the statistical distribution of Residence Times and Shear Stress Histories experienced by platelets in those trajectories.

3.1.3 Platelet residence times (RT) and stress histories (SH)—RT is calculated for every platelet from its time of injection to the time it exits the domain (or until the

simulation ends). SH is calculated for every platelet, by cumulative addition of the values of shear stress that the platelet is exposed to, for the entire time that the platelet is circulating in the region of interest.

A total of over 150,000 platelets were released from the inlet over 10 cardiac cycles for each configuration. We focus our analyseson theparticles traveling towards the brain (comprising of particles that exit through the brachiocephalic, carotid and subclavian branches), in an effort to provide insights into the risk of stroke associated with blood flow features caused by the LVAD outflow graft configuration.

The lowest median RT (0.36 s) is found for the 60° configuration, while particles remained significantly longer in the domain (0.64 s) for the 90° configuration (with those in the 45° configuration very close to the 60° value, at 0.39 s). The PDF plot in Figure 6(a) indicates that a large amount of particles for the 90° configuration had lingered in the aortic arch region longer than the other configurations. PO plots indicate that particles for the 90° configuration have a ~ 150% higher risk of lingering in the vasculature longer than 1 s. The % of outliers with high RT and high SH was largest for the 90° configuration: 16.21% for RT and 12.08% for SH, while the values are minimum for 60° and 45° respectively.

Table 2 shows the median and outlier information for all particles traveling towards the brain.

Figure 6(b) shows PDF, boxplot and PO plots of SH traveling towards the brain. Particles had the lowest median SH (0.54 Pa-s) in the 60° configuration, whereas they accumulated the highest stress histories (0.91 Pa-s) for the 90° configuration. The 45° configuration had close but higher values than the 60° case, at 0.63 Pa-s. The probability distribution (PDF) clearly indicates that a significant number of particles for the 90° configuration had a high probability of SH between 0.5 and 2 Pa-s, physiologically relevant values. These particles accumulate ~70% higher SH compared to the other two lower angle configurations. PO plots indicate that particles for the 90° configuration have a ~ 55% higher risk of accumulating a SH between 1 and 2 Pa-s compared to the 45° configuration, and an overall ~ 67% higher risk of accumulating a SH higher than 1 Pa-s. The maximum SH was attained by particles in the 90° configuration (133.95 Pa-s) which was ~12% higher than for particles in the 45° configuration. The % of outliers was also largest for the 90° configuration (12.08%). Table 2 shows the detailed SH statistics.

The particles that travel towards the upper body can be further classified based on the artery that they flow into: brachiocephalic, left common carotid or left subclavian. Overall, RT and SH of particles exiting the brachiocephalic, carotid and subclavian were highest for the 90° configuration, indicating higher thrombogenic potential. Similarly, when the analysis was extended to all particles in the domain, regardless of whether they have left the domain in the simulation time, or where they left towards, the results were fully consistent with the previous discussion: the 90° configuration presented higher RT and SH values, with a statistically significant increase in the number of particles that suffered from very large residence times and shear stress histories, compared to the two shallower angle

configurations, 45° and 60°. Further risk analysis based on the platelet history and thrombogenic potential can be found in the Supplementary Materials.

3.2 Eulerian Hemodynamic Parameters

3.2.1 Wall Shear Stress (WSS)—Figure 7 shows the WSS distributions on the ascending aorta, aortic arch, great vessel ostia and descending aorta. It can be clearly seen that there are high levels of WSS on the posterior region of the aortic arch, just proximal to the brachiocephalic branch. This high WSS zone is associated with the impingement of the high-velocity jet from the outflow graft. As the outflow graft is best aligned with the anatomy of the ascending aorta for the 45° configuration, the WSS peak values are lower in this case, the area under high WSS is smaller, and it is more distal, close to the ostia of the brachiocephalic branch and carotid artery (see posterior view in Figure 7). Interestingly, the WSS on the brachiocephalic ostium increases from the 45° configuration to the 60° configuration, and then decreases for the 90° configuration. Overall, no singular outflow graft angle configuration globally minimizes the WSS on the arterial walls, but there are important localized differences that are physiologically significant in dislodging thrombi that may temporarily nest and grow at the ostia of the cerebral vasculature.

3.3 Evaluation of minimum thrombogenic potential (MTP)

TP was evaluated for particles traveling towards the brain for the three configurations studied, in order to evaluate their overall thrombogenic performance. Based on the criteria specified in section 2.6, the scores assigned to the various configurations are shown in Table 3. Overall, the 90° configuration was the most thrombogenic, with a maximum values of the mean residence time and mean and maximum shear stress histories. Additionally, this configuration produces significantly higher percentage of outliers (platelets that withstand RT and SH values 2.5 times the standard deviation higher than the median in the best configuration) resulting in the maximum normalized TP score of 0.85. The 60° configuration was least thrombogenic (score of 0.2), with the 45° yielding a very close normalized TP score of 0.3, indicating similar thrombogenic performance for the acute angles studied.

4 DISCUSSION

In this work, we present a methodology to assess thrombogenic potential of various LVAD outflow graft configurations. We focus on understanding thrombogenicity of the blood flow features created by different LVAD outflow graft configurations, using Lagrangian metrics for platelet surrogates traversing the aortic arch. The hemodynamic environment studied here is assessed for its impact on the coagulation cascade's natural equilibrium of thrombogenic and anti-thrombogenic factors, in a way that aims to predict growth of microthrombi, originating from the LVAD, or formation of clots due to activated platelets and thrombin strands originating entirely post-VAD. Just like as our study is device neutral, it does not establish specific location of thrombus initiation, as the goal is to predict the fate of particles representing an organized thrombus or an incipient thrombus forming as platelets find the conditions to activate and accumulate in circulation, as the sequelae of unfavorable device biocompatibility.

The most significant methodological innovation of this study is the comprehensive use of Lagrangian metrics to elucidate the hemodynamic environment experienced by platelets navigating the aortic. Hundreds of thousands of particles were released from the outflow graft every 1/10 seconds and their motion and stress accumulation tracked continuously. Particle trajectories indicate particles are trapped in recirculation zones and in swirling flows as shown in Figures 3 and 5. The trapping of particles in recirculation zones leads to particles spending longer time in the aortic arch, before being transported to the distal circulation. Long residence times are a necessary step towards agglomeration after flow-induced platelet activation[38,39, 41]. While the average time taken by particles to traverse the aortic arch and exit the brachiocephalic branch was ~ 0.28 seconds for the 45° and 60° configurations, particles were in the aortic territory for ~ 0.5 second before exiting the brachiocephalic branch for the 90° configuration (a 71% increase). Increases in particle RT were also observed for particles exiting the subclavian (66%) and carotid branches (20%) for the 90° configurations. Particle RT analyses indicates that the 90° configuration is potentially more thrombogenic on account of particles being trapped in the aortic root region for much longer times. Some of these particles are trapped in the recirculating zone just distal to the aortic valve in the aortic root, potentially increasing the risk of aortic valve damage or thrombosis.

Shear-induced-platelet-activation[12,36–40] has been the focus of many studies in evaluating thrombogenesis of medical devices[23,42]. In this study, we have quantified levels of shear stress histories on individual platelets to evaluate the relative thrombogenicity of LVAD outflow graft configurations. Platelet SH data indicate a trend similar to particle RT. Accumulated SH for particles is lower for the 45° and 60° configurations, with a majority of particles accumulating a <~ 0.75 Pa-s shear history. However, for the 90° configuration, particles accumulated > 1 Pa-s SH (a >45% increase). These results indicate that the 90° configuration is clearly most unfavorable, with particles accumulating elevated SH and consequently elevated risk of SIPA. This trend was similarly found for the platelet maximum SH, with particles in the 90° configuration reaching a maximum accumulated SH (134 Pa-s), compared to 121 Pa-s for the 60°configuration and 120 Pa-s for the 45° configuration.

Especially important is the combination of strong recirculation regions coupled with increased RT and SH, as these may lead to conditions conducive to platelet activation and thrombus initiation. Moreover, the 90° configuration resulted in particles accumulating larger SH prior to exiting the brachiocephalic (~ 12% increase) and the carotid (~ 70% increase) arteries. These results provide valuable insights into the propensity of LVAD patients to experience cerebrovascular events rather than embolize to visceral or peripheral circulation[53].

It is important to note that all three configurations presented outlier particles for both RT and SH analyses, and these may be critical for thrombus initiation. Consistent with previous discussion, the % outliers for particle RT was highest for the 90° configuration (16%) in comparison to the 60° configuration (8%) and 45° configuration (12%). The % of outliers (RT, SH) was also highest for the 90° configuration when particles were subcategorized into the brachiocephalic (43.94%, 25.41%) and the subclavian (17.34%, 18.14%) arteries. The outlier analysis indicates that 90° configuration results in complex hemodynamic patterns

and flow recirculation zones, leading to very large SH accumulation, combined with high RT in some, but not all, cases.

As shown in Table 3, the median and outlier information for RT and SH were used in evaluating TP for all three outflow graft configurations. Maximum values of median and outliers did not always occur for the 90° configuration; five of six categories (all except maximum RT value) were highest for the 90° configuration. Overall, the 45° and 60° configurations had lowest scores in two and three out of six metrics, respectively, but those resulted in the lowest overall TP scores. It is important to note that this analysis clearly indicates all configurations present some platelet outliers that may alone create thrombogenic risk, importantly noting the 90° configuration is *most* thrombogenic, while the 45° and 60° configurations being more favorable for thrombogenic potential.

While evaluating the thrombogenic potential of the three configurations tested in this study, it is important to consider particle density. Despite analyzing > 150,000 particles for each configuration over the duration of the simulations, the particle density in our simulations is ~ 200 particles/mL. In actuality, the platelet density of human blood under normal conditions is ~ 250×10^6 platelets/mL[35], an increase by a factor of 10^6. This relative density factor has major implications for evaluating outliers, as every outlier is representative of ~10^6 platelets. The outlier particles in our simulation continue to circulate within the computational domain for over 10 seconds, in the process accumulating high values of SH. The outliers for particle SH for the 90° configuration (~150 Pa-s) could potentially indicate many millions of platelets not only circulating for well over 10 seconds, but also accumulating non-physiologically high SH. This markedly increases the risk of platelets activating soon after entering the aortic circulation and having long times to accumulate before traveling towards the brain, thus exacerbating stroke risk.

Continuous VAD flow through a fixed-diameter outflow graft creates a high-velocity jet of blood as it exits the graft and impinges on the contralateral aortic wall in the ascending aorta (see Figure 3). An immediate consequence of the impingement of the jet is an associated region of high WSS on the posterior aortic wall that remains nearly constant for the duration of the simulations. As the high-velocity jet impinges on the posterior wall, it breaks down into chaotic recirculating eddies moving blood around the entire aortic root and towards the anterior wall, leading to another region of moderately elevated WSS. The WSS on the posterior ascending aorta is reduced for the more acute (45° and 60°) configurations, while the brachiocephalic branch is exposed to higher WSS at 45° and 60° than the 90° configuration. Most importantly, the impingement zone in the contralateral aortic wall experiences a nearly constant WSS of more than 10 Pa, while the WSS on the majority of the aortic arch and the descending aorta is less than 2 Pa. This highly heterogeneous WSS distribution coupled with a constant exposure of high WSS in a small region of the aortic arch can strongly influence endothelial cell function and arterial wall health[43–45]. Other research groups have also found regions of elevated WSS at the location of LVAD graft outflow impingement[25,29, 30,46,47]. While the more acute angles reduce the WSS maximum on the aorta and increases the values near the brachiocephalic and carotid ostia, possibly reducing the risk of endothelial dysfunction in the aortic root and the temporary lodging of

microthrombi at the upper body arterial bifurcations before leaving as larger thrombus, no single configuration globally minimizes WSS on the arterial walls.

The blood flow exiting the outflow graft, after impingement as a jet onto the aortic wall, gives rise to a swirling and recirculation zone, as shown in Figure 3. The LVAD outflow graft flow experiences less swirling motion and recirculation for the 45° and 60° configurations, due to the better alignment of the momentum of the jet with the axis of the aorta. The farther reach of the high-speed flow from the outflow graft in the 45° and 60° configurations, however, results in higher WSS on the ostia of the brachiocephalic branch and left carotid artery. Swirling flow is observed in the aortic arch for all outflow graft configurations, but the hemodynamics of the 90° configuration are dramatically more chaotic; with multiple high-speed swirls breaking off from the primary jet upon impingement on the posterior ascending aorta. One of these streams forms a large recirculating zone in the aortic root, and in the absence of aortic valve opening, takes platelets into a stagnation region where they have the potential to agglomerate after activation. Further, this retrograde recirculation zone displays relatively high pressure, due to stagnation, and may influence aortic valve regurgitation, possibly by exacerbating aortic valve damage over time[48–51].

4.1 LIMITATIONS

The current study quantifies hemodynamic performance and thrombogenic potential of various outflow graft anastomoses configurations using state-of-the-art Lagrangian metrics. However, it is not without limitations.

Firstly, the vascular and graft walls were considered to be rigid, simplifying the dynamics of flow in the vasculature. Several studies have shown that, while wall compliance modifies flow stresses and features quantitatively by about 10–20%, it does not modify the qualitative effects of vascular anatomy and in particular, it does not change the risk stratification of multiple computed cases with the same assumption, as compliance affects all cases similarly[52]. The constant shape of the outflow graft, assumed to be unaffected by pressure-induced dilatation and the remote possibility of long-term remodeling, is consistent with the behavioral properties of commercially-used contemporary VAD outflow grafts. However, if any change of cross-sectional area or angle at the anastomosis due to graft elasticity or remodeling (larger cross sectional area or higher incidence angle, as it would occur if the graft deformed into a cuffed shape) were to occur, it would be directed towards reducing the longitudinal momentum injected at the aorta. The hemodynamic impact of this, increasing platelet residence time, would exacerbate the risk of thrombosis in all configurations.

The effect of age and stage of vascular health in an LVAD population would lead to a significantly reduced arterial compliance, and the diminished pulsatility in continuous flow LVAD circulation would further support this assumption. More importantly, only one patient vasculature was simulated in this study. While the anatomy and flow rates are representative of the population of interest, a range of patient-specific models should be simulated to confirm the trends in this study are robust for most, if not all, the possible anatomical or physiological (flow rates and peripheral resistances) variations. This study is intentionally device-neutral and, because of this, does not explore in detail subtle differences in flow

inherent to centrifugal and axial designs. Our study uses boundary conditions based on physiological flow rates measured at locations downstream of the aortic arch, and thus cannot take into account the vastly different P-Q curves of axial and centrifugal pumps, and the CFD methodology does not adapt itself to taking arterial compliance without Fluid-Structure Interaction simulations. In a part of the study not shown, we confirmed that the rotational flow exiting the pump at the inlet to the outflow graft did not qualitatively change flow patterns at the aortic root, as the rotational component of the flow (± 20% of the streamwise velocity) had broken down into incoherent vorticity patches that play a role in transition to turbulence in the graft itself but become negligible at the anastomosis.

5 CONCLUSION

This study presents a novel, comprehensive, device-neutral analysis methodology, investigating platelet residence time/shear stress (platelet-level) and wall shear stress (endothelial-level) metrics able to quantify hemodynamic complications and relative thrombogenic risk of different surgical configurations.

Our simulations demonstrate that shallower angles result in favorable hemodynamics and reduced thrombogenicity in the aortic arch and cerebral vessel bifurcations. The 45° and 60° configurations were found *least* thrombogenic (with very similar risk values), while the 90° configuration was *most* thrombogenic. We also quantified specific hemodynamics pertinent to stroke risk: (i) increases in particle RT were observed for particles flowing to the brachiocephalic (~71% increase), subclavian (~66% increase) and left carotid arteries (~20% increase) for the 90° configuration and (ii) there was a ~45% increase in particle SH for the 90° configuration with increases in particle SH observed specifically for platelets flowing through the brachiocephalic (~ 12% increase) and the left carotid (~ 70% increase) branches. While more research is needed to determine the influence of varying blood flow patterns in the aortic arch region on platelets and their subsequent activation state, incorporating Lagrangian (platelet level) metrics to the traditional Eulerian Wall Shear Stress enables deeper understanding of LVAD hemodynamics and subsequently facilitate thrombogenic assessment of implantation configurations. These findings suggest that outflow graft angles in the 45–60° range may mitigate thrombogenic potential by reducing platelet activation in the ascending aorta. This may favorably impact LVAD outcomes by reducing the risk of neurologic events related to platelet activation at the outflow graft anastomosis. Further clinical evaluation of variable outflow graft angulation is warranted to guide surgical planning.

Supplementary Material

Refer to Web version on PubMed Central for supplementary material.

Acknowledgments

CONFLICT OF INTEREST STATEMENTS

The authors would like to thank the High Performance Computing (HPC) group for providing the high performance computing facility (Hyak) at the University of Washington to conduct the simulations described in this study.

Conflicts of interest: NAM has a consulting relationship with St. Jude and HeartWare, and is an investigator for St. Jude, HeartWare, and SynCardia. CM has consulting relationships with Thoratec St. Jude, Abiomed and HeartWare and is an investigator for St. Jude, HeartWare, and SynCardia, JB has consulting relationships with Abiomed, HeartWare and Thoratec St. Jude.

REFERENCES

1. Mozaffarian D, Benjamin EJ, Go AS, et al. Heart disease and stroke statistics-2015 update: A report from the American Heart Association. 2015
2. Go AS, Mozaffarian D, Roger VL, et al. Heart Disease and Stroke Statistics-- 2014 Update: A report from the American Heart Association. 2014
3. Mancini D, Colombo PC. Left Ventricular Assist Devices: A Rapidly Evolving Alternative to Transplant. J Am Coll Cardiol. 2015; 65:2542–2555. [PubMed: 26065994]
4. Heidenreich PA, Albert NM, Allen LA, et al. Forecasting the impact of heart failure in the United States: a policy statement from the American Heart Association. Circ Heart Fail. 2013; 6:606–19. [PubMed: 23616602]
5. Allen LA, Stevenson LW, Grady KL, et al. Decision making in advanced heart failure: A scientific statement from the american heart association. Circulation. 2012; 125:1928–1952. [PubMed: 22392529]
6. Crespo Leiro MG, Paniagua Martin MJ. [Management of advanced or refractory heart failure]. Rev Esp Cardiol. 2004; 57:869–883. [PubMed: 15373993]
7. Mulloy DP, Bhamidipati CM, Stone ML, Ailawadi G, Kron IL, Kern Ja. Orthotopic heart transplant versus left ventricular assist device: a national comparison of cost and survival. J Thorac Cardiovasc Surg. 2013; 145:566–573. discussion 573–4. [PubMed: 23246055]
8. Miller LW, Pagani FD, Russell SD, et al. Use of a continuous-flow device in patients awaiting heart transplantation. N Engl J Med. 2007; 357:885–896. [PubMed: 17761592]
9. Slaughter MS, Rogers JG, Milano Ca, et al. Advanced heart failure treated with continuous-flow left ventricular assist device. N Engl J Med. 2009; 361:2241–2251. [PubMed: 19920051]
10. Slaughter MS, Pagani FD, McGee EC, et al. HeartWare ventricular assist system for bridge to transplant: Combined results of the bridge to transplant and continued access protocol trial. J Hear Lung Transplant. 2013; 32:675–683.
11. Jorde UP, Kushwaha SS, Tatooles AJ, et al. Results of the Destination Therapy Post-FDA-Approval Study with a Continuous Flow Left Ventricular Assist Device: A Prospective Study Using the INTERMACS Registry. J Am Coll Cardiol. 2014; 63
12. Najjar SS, Slaughter MS, Pagani FD, et al. An analysis of pump thrombus events in patients in the HeartWare ADVANCE bridge to transplant and continued access protocol trial. J Heart Lung Transplant. 2014; 33:23–34. [PubMed: 24418731]
13. Rogers JG, Aaronson KD, Boyle AJ, et al. Continuous flow left ventricular assist device improves functional capacity and quality of life of advanced heart failure patients. J Am Coll Cardiol. 2010; 55:1826–1834. [PubMed: 20413033]
14. Mehra MR, Stewart GC, Uber Pa. The vexing problem of thrombosis in long-term mechanical circulatory support. J Hear Lung Transplant. 2014; 33:1–11.
15. Kirklin JK, Naftel DC, Pagani FD, et al. Sixth INTERMACS annual report: A 10,000-patient database. J Hear Lung Transplant. 2014; 33:555–564.
16. Starling RC, Moazami N, Silvestry SC, et al. Unexpected Abrupt Increase in Left Ventricular Assist Device Thrombosis. N Engl J Med. 2014; 370:33–40. [PubMed: 24283197]
17. Lampropulos JF, Kim N, Wang Y, et al. Trends in left ventricular assist device use and outcomes among Medicare beneficiaries, 2004–2011. Open Hear. 2014; 1:e000109.
18. Willey J, Boehme A. Hypertension and Stroke in Patients with Left Ventricular Assist Devices (LVADs). Curr Hypertens …. 2016
19. Schmid C, Weyand M, Nabavi D. Cerebral and systemic embolization during left ventricular support with the Novacor N100 device. Ann Thorac …. 1998
20. Morgan J, Brewer R, Nemeh H. Stroke while on long-term left ventricular assist device support: incidence, outcome, and predictors. ASAIO …. 2014

21. Tsukui H, Abla A, Teuteberg J. Cerebrovascular accidents in patients with a ventricular assist device. J Thorac …. 2007
22. Xenos M, Girdhar G, Alemu Y, et al. Device Thrombogenicity Emulator (DTE)--design optimization methodology for cardiovascular devices: a study in two bileaflet MHV designs. J Biomech. 2010; 43:2400–2409. [PubMed: 20483411]
23. Bluestein D, Chandran K, Manning K. Towards non-thrombogenic performance of blood recirculating devices. Ann Biomed Eng. 2010; 38:1236–1256. [PubMed: 20131098]
24. Chandran, K.; Rittgers, S.; Yoganathan, A. Biofluid mechanics: the human circulation. CRC Press; 2012.
25. Karmonik C, Partovi S, Schmack B, et al. Comparison of hemodynamics in the ascending aorta between pulsatile and continuous flow left ventricular assist devices using computational fluid dynamics based on computed tomography images. Artif Organs. 2014; 38:142–148. [PubMed: 23889366]
26. Farag MB, Karmonik C, Rengier F, et al. Review of Recent Results Using Computational Fluid Dynamics Simulations in Patients Receiving Mechanical Assist Devices for End-Stage Heart Failure. Methodist Debakey Cardiovasc J. 2014; 10:185–189. [PubMed: 25574347]
27. Karmonik C, Partovi S, Loebe M, et al. Computational fluid dynamics in patients with continuous-flow left ventricular assist device support show hemodynamic alterations in the ascending aorta. J Thorac Cardiovasc Surg. 2014; 147:1326.e1–1333.e1. [PubMed: 24345553]
28. Osorio AF, Osorio R, Ceballos A, et al. Computational fluid dynamics analysis of surgical adjustment of left ventricular assist device implantation to minimise stroke risk. Comput Methods Biomech Biomed Engin. 2013; 16:622–638. [PubMed: 22185643]
29. Karmonik C, Partovi S, Loebe M, et al. Influence of LVAD cannula outflow tract location on hemodynamics in the ascending aorta: a patient-specific computational fluid dynamics approach. ASAIO J. 2012; 58:562–567. [PubMed: 23013842]
30. May-Newman K, Hillen B, Dembitsky W. Effect of left ventricular assist device outflow conduit anastomosis location on flow patterns in the native aorta. ASAIO J. 2006; 52:132–139. [PubMed: 16557097]
31. Ong C, Dokos S, Chan B, et al. Numerical investigation of the effect of cannula placement on thrombosis. Theor Biol Med Model. 2013; 10:35. [PubMed: 23680359]
32. Bazilevs Y, Gohean JR, Hughes TJR, Moser RD, Zhang Y. Patient-specific isogeometric fluid-structure interaction analysis of thoracic aortic blood flow due to implantation of the Jarvik 2000 left ventricular assist device. Comput Methods Appl Mech Eng. 2009; 198:3534–3550.
33. Mazzitelli R, Boyle F, Murphy E, Renzulli A, Fragomeni G. Numerical prediction of the effect of aortic Left Ventricular Assist Device outflow-graft anastomosis location. Biocybern Biomed Eng. 2016:1–17.
34. LaDisa JF, Dholakia RJ, Figueroa CA, et al. Computational Simulations Demonstrate Altered Wall Shear Stress in Aortic Coarctation Patients Treated by Resection with End-to-end Anastomosis. Congenit Hear Dis. 2011; 6:432–443.
35. Widmaier, E.; Raff, H.; Strang, K. Vander's human physiology: the mechanisms of human body function. McGraw-Hill; 2006.
36. Shankaran H, Alexandridis P, Neelamegham S. Aspects of hydrodynamic shear regulating shear-induced platelet activation and self-association of von Willebrand factor in suspension. Blood. 2003; 101:2637–2645. [PubMed: 12456504]
37. Sheriff J, Soares JS, Xenos M, Jesty J, Bluestein D. Evaluation of shear-induced platelet activation models under constant and dynamic shear stress loading conditions relevant to devices. Ann Biomed Eng. 2013; 41:1279–1296. [PubMed: 23400312]
38. Para, a; Bark, D.; Lin, a; Ku, D. Rapid platelet accumulation leading to thrombotic occlusion. Ann Biomed Eng. 2011; 39:1961–1971. [PubMed: 21424850]
39. Einav S, Bluestein D. Dynamics of blood flow and platelet transport in pathological vessels. Ann N Y Acad Sci. 2004; 1015:351–366. [PubMed: 15201174]
40. Chesnutt JKW, Han H-C. Computational simulation of platelet interactions in the initiation of stent thrombosis due to stent malapposition. Phys Biol. 2016; 13:016001. [PubMed: 26790093]

41. Ramstack JM, Zuckerman L, Mockros LF. Shear-induced activation of platelets. J Biomech. 1979; 12:113–125. [PubMed: 422576]
42. Bluestein D, Yin W, Affeld K, Jesty J. Flow-induced platelet activation in a mechanical heart valve. J Hear Valve …. 2004
43. Dolan JM, Meng H, Singh S, Paluch R, Kolega J. High fluid shear stress and spatial shear stress gradients affect endothelial proliferation, survival, and alignment. Ann Biomed Eng. 2011; 39:1620–1631. [PubMed: 21312062]
44. Davies PF. Hemodynamic shear stress and the endothelium in cardiovascular pathophysiology. Nat Clin Pract Cardiovasc Med. 2009; 6:16–26. [PubMed: 19029993]
45. Malek AM, Alper S, Izumo S. Hemodynamic Shear Stress and Its Role in Atherosclerosis. JAMA. 1999; 282:2035. [PubMed: 10591386]
46. Inci G, Sorgüven E. Effect of LVAD Outlet Graft Anastomosis Angle on the Aortic Valve, Wall, and Flow. ASAIO J. 2012; 58:373–381. [PubMed: 22739783]
47. Brown AG, Shi Y, Arndt A, Müller J, Lawford P, Hose DR. Importance of realistic LVAD profiles for assisted aortic simulations: evaluation of optimal outflow anastomosis locations. Comput Methods Biomech Biomed Engin. 2012; 15:669–680. [PubMed: 21409657]
48. Samuels LE, Thomas MP, Holmes EC, et al. Insufficiency of the native aortic valve and left ventricular assist system inflow valve after support with an implantable left ventricular assist system: Signs, symptoms, and concerns. J Thorac Cardiovasc Surg. 2001; 122:380–381. [PubMed: 11479514]
49. Cowger J, Pagani F, Haft J. The development of aortic insufficiency in left ventricular assist device-supported patients. … Hear Fail. 2010
50. Aggarwal A, Raghuvir R, Eryazici P. The development of aortic insufficiency in continuous-flow left ventricular assist device–supported patients. Ann Thorac …. 2013
51. Pak S, Uriel N, Takayama H. Prevalence of de novo aortic insufficiency during long-term support with left ventricular assist devices. J Hear …. 2010
52. McGah P, Leotta D, Beach K, Aliseda A. Effects of wall distensibility in hemodynamic simulations of an arteriovenous fistula. Biomech Model. 2014
53. Kirklin JK, Naftel DC, Pagani FD. Seventh INTERMACS annual report: 15,000 patients and counting. J. Heart Lung Transplant.
54. McGah PM, Leotta DF, Beach KW, Zierler RE, Aliseda A. Incomplete restoration of homeostatic shear stress within arteriovenous fistulae. J Biomech Eng. 2013; 135

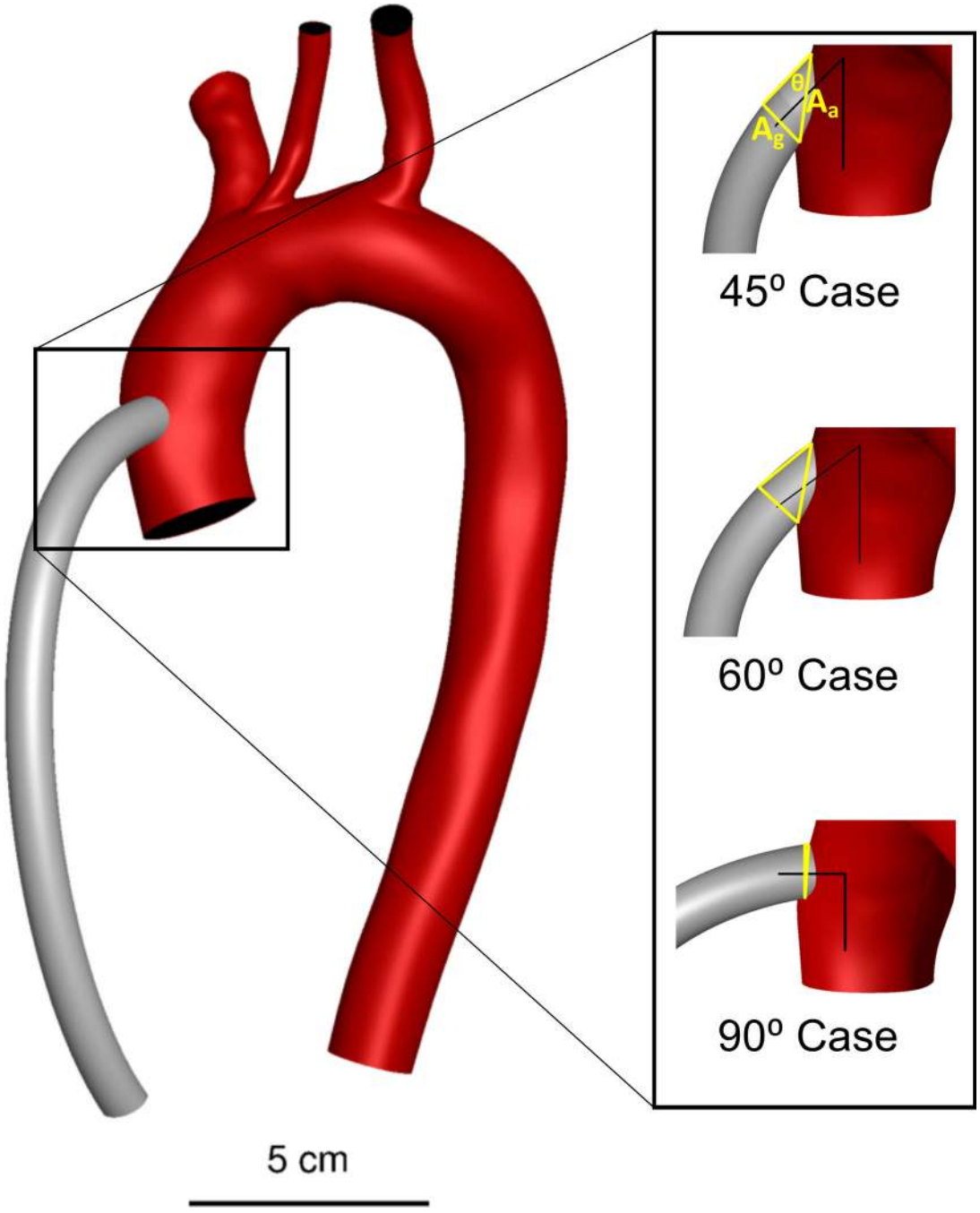

Figure 1.

Patient-specific model of aorta and great vessel branches with a 10 mm outflow graft (grey), three virtually anastomosed outflow graft configurations. The triangles in yellow represent the anastomotic area as a function of the graft cross sectional area and the anastomosis angle, an upper limit of the area over which a highly distensible graft could spread the momentum entering the aorta in the case of dilatation or remodeling.

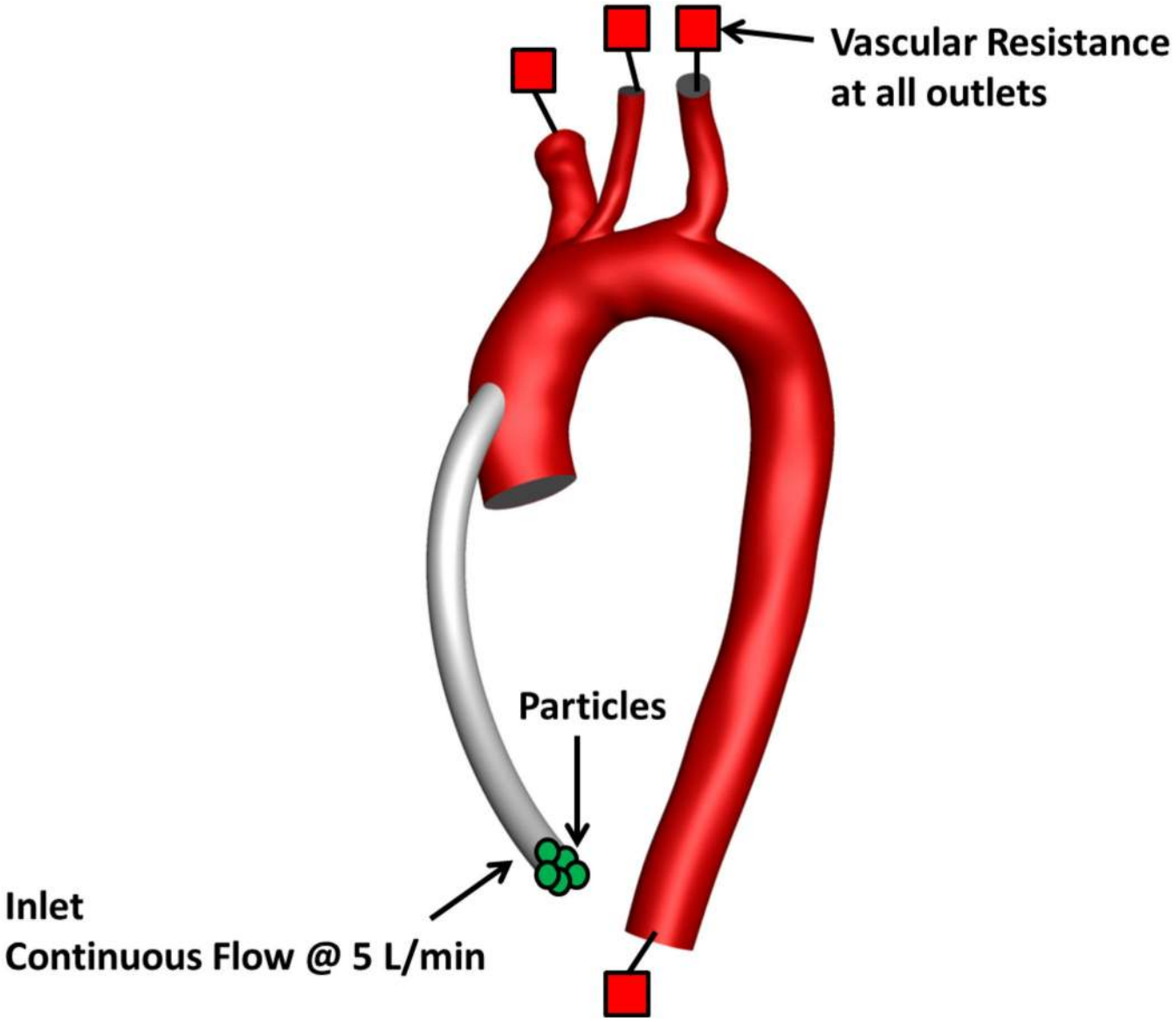

Figure 2.
Computational domain and boundary conditions

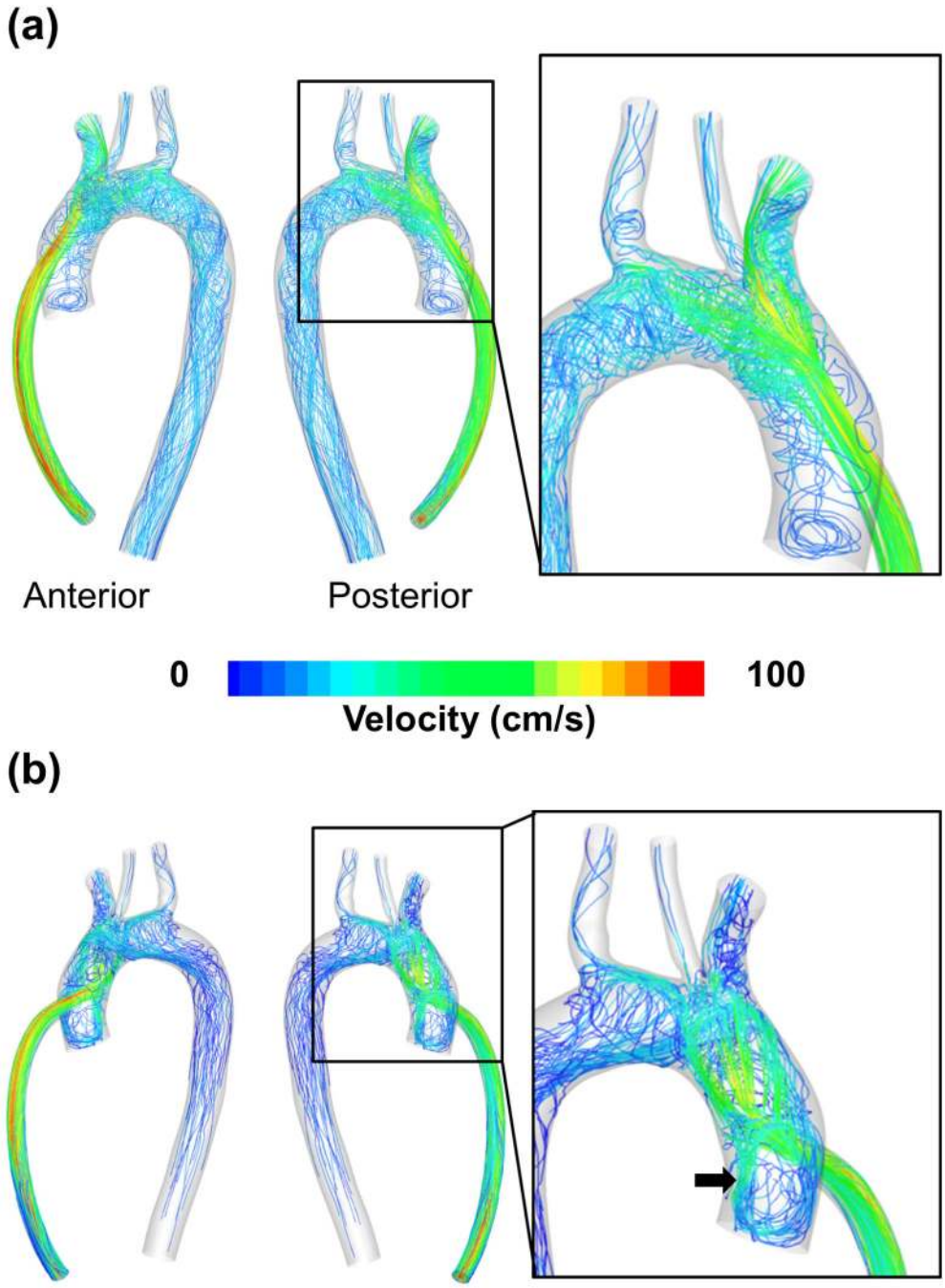

Figure 3.

(a) Hemodynamic flow patterns for 60° case (b) Hemodynamic flow patterns for the 90° case. For the 90° case, the splitting of the high-velocity jet from the outflow graft into multiple streams, and a strong recirculation zone just distal to the aortic valve is clearly seen (black arrow)

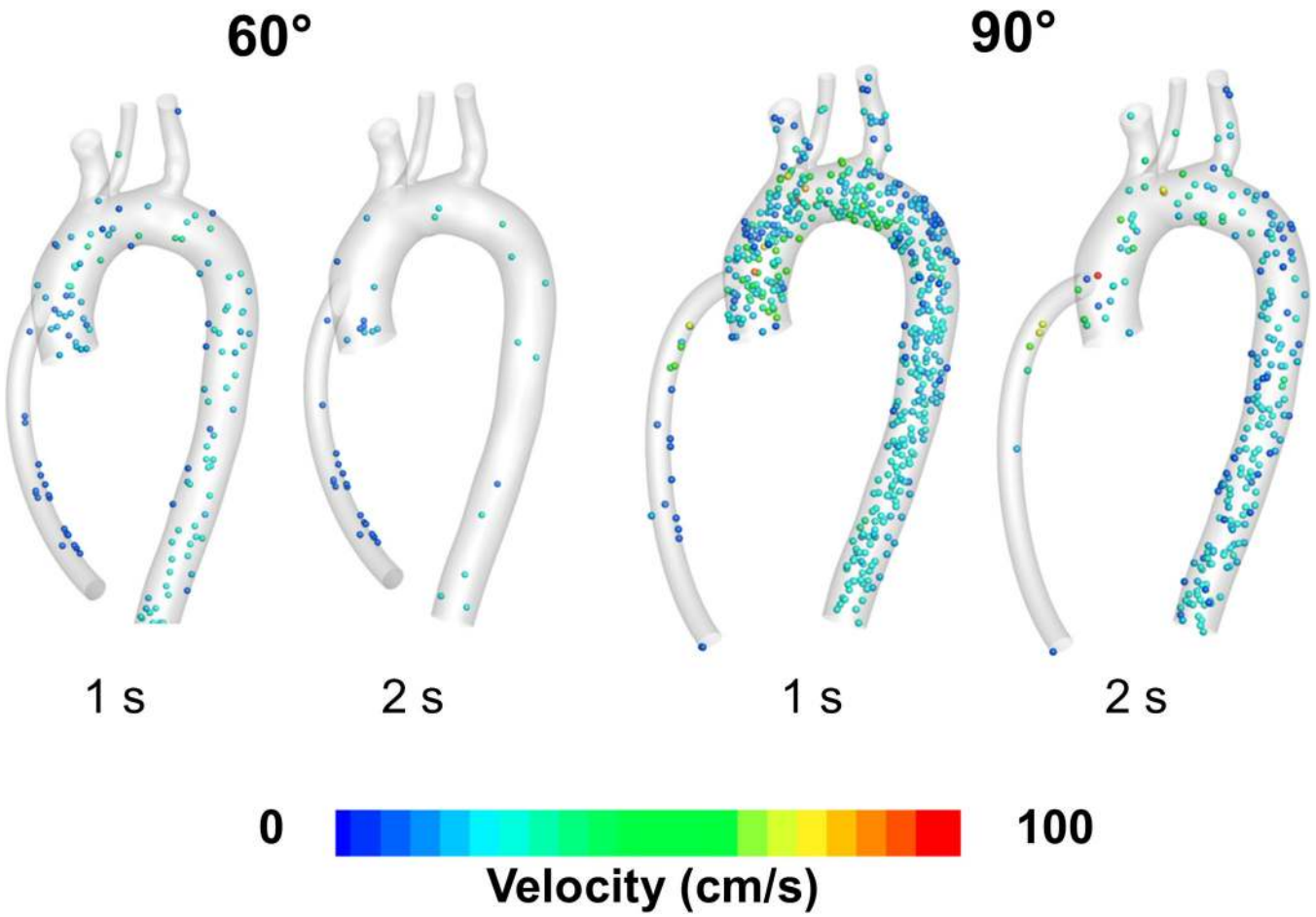

Figure 4.
Snapshot showing particles circulating in the aortic region, 1 and 2 seconds after injection for the 60° and 90° cases

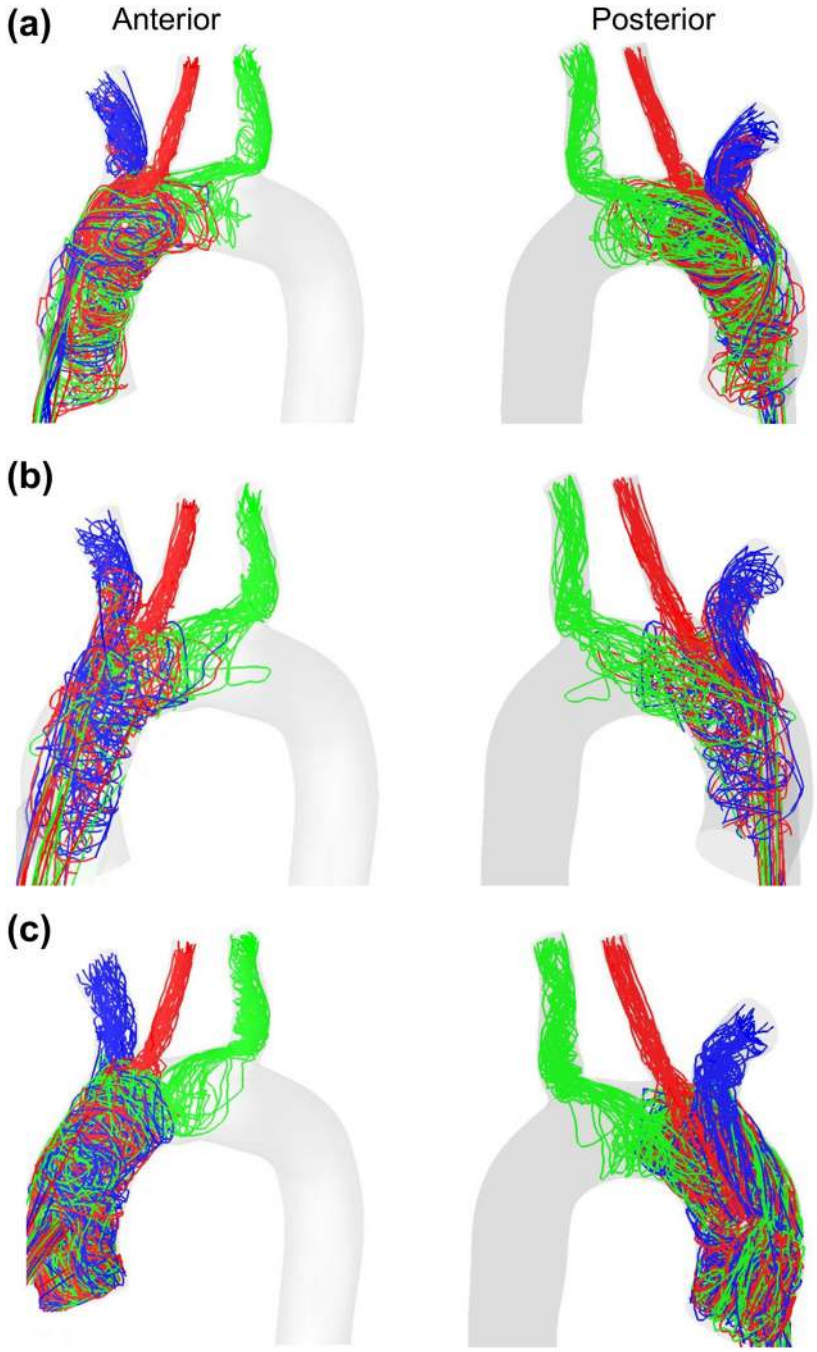

Figure 5.

Platelet trajectories for the (a) 45° configuration, (b) 60° configuration and (c) 90° configuration. Trajectories are plotted for ~ 30 platelets exiting through each of the brachiocephalic (blue), left common carotid (red) and left subclavian (green) arteries. Outflow graft not shown for simplicity.

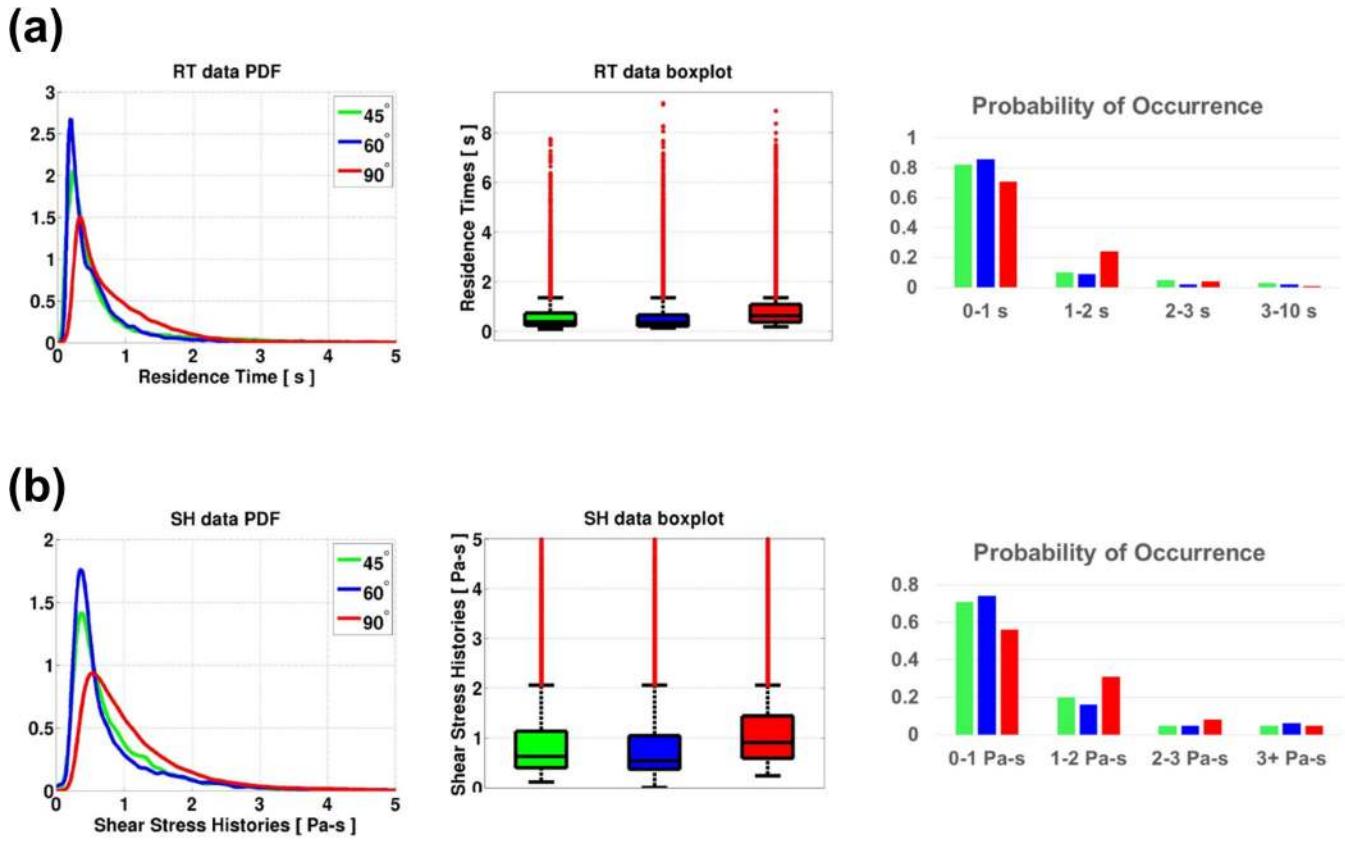

Figure 6.
PDF, boxplot and PO plots of (a) RT and (b) SH for all particles traveling towards the brain.

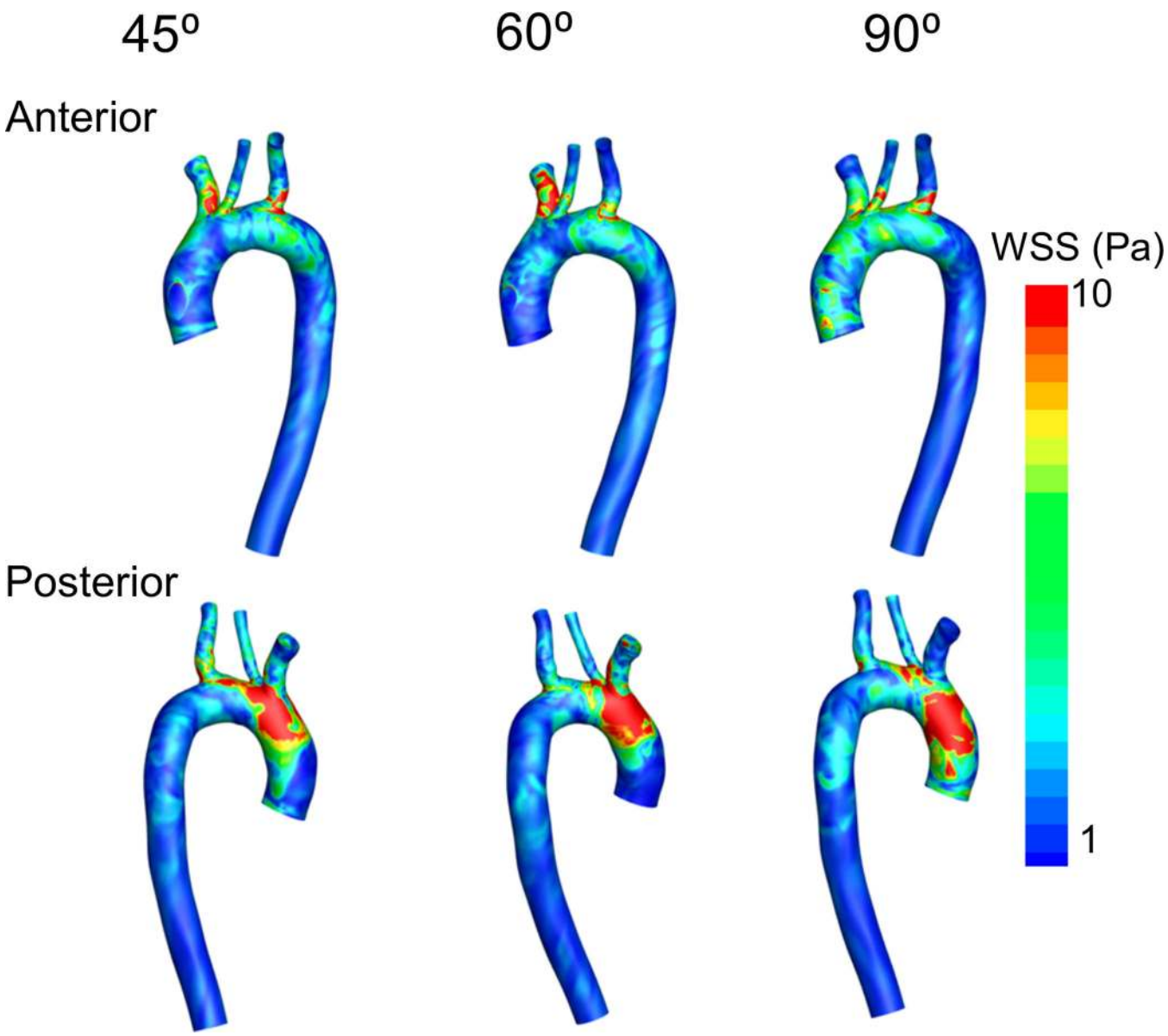

Figure 7.
WSS on arterial walls for all three configurations. Outflow graft not shown

Table 1

Criteria used for evaluation of TP

RT (50%)			SH (50%)		
Median	**Outlier Max (maximum value)**	**Outlier % (% of data that are outliers)**	**Median**	**Outlier Max (maximum value)**	**Outlier % (% of data that are outliers)**
25%	15%	10%	25%	15%	10%

Table 2

Median and outlier information of RT and SH for particles traveling towards the brain.

Case	Residence Time (s)		Stress Histories (Pa-s)	
	Median	Outliers (Max, %)	Median	Outliers (Max, %)
45 °	0.39 †‡	8.89, 12.70%	0.63 †‡	119.54, 9.04%
60 °	0.36 *‡	9.19, 7.88%	0.54 *‡	120.84, 10.03%
90 °	0.64 *†	7.76, 16.21%	0.91 *†	133.95, 12.08%

(Note:

*indicates a statistically significant ($p < 0.05$) result in comparison with 45 ° configuration,

†indicates a statistically significant ($p < 0.05$) result in comparison with 60° configuration and

‡indicates a statistically significant ($p < 0.05$) result in comparison with 90° configuration.)

Table 3

Evaluation of TP for all three outflow graft configurations

CASE	RT scores			SH scores			TP
	Median	Outlier Max	Outlier %	Median	Outlier Max	Outlier %	
45°	0.11	0.79	0.58	0.24	0.00	0.00	**0.29**
60°	0.00	1.00	0.00	0.00	0.09	0.33	**0.20**
90°	1.00	0.00	1.00	1.00	1.00	1.00	**0.85**